Reviewer #1

The study uses a multi-step approach that identifies physics parameters that are most influential to MJO simulation skill, proposes a parameter set that produces a much improved MJO compared to the default parameter set, links parameter adjustments to physical processes, and demonstrates that the tuned parameter set does not also degrade the time mean of precipitation. Results from a perturbed parameter ensemble (PPE), similar to those of previous studies, are fed to a generalized linear model (GLM) that identifies *dmpdz*, *tau*, and *ai* as the most impactful parameters for MJO simulation skill. A final perturbed experiment "DTE" in which *dmpdz* is maximized and *ai* and *tau* are minimized (as suggested by the GLM results) exhibits a considerably improved MJO relative to the control run "CTL". The authors use the moist static energy (MSE) budget to link the parameter adjustments to physical mechanisms that favor MJO improvement:

(1) *dmpdz* improves the climatological moisture distribution (particularly the meridional gradient) on which MJO circulation anomalies act to promote MJO eastward propagation, and (2) *ai* improves cloud-radiation feedbacks (and thus MJO maintenance) by increasing the amount of ice cloud produced per unit precipitation.

The specific influence of parameter *tau* remains unclear. The parameter changes in DTA do not degrade the time mean precipitation relative to CTL, but the impact on other state fields in DTA was not examined. Reconsider after major revisions. The text is logically organized, the figures are easily understood, and the scientific interpretation of the results is generally sound. Although PPE, GLA, and the MSE budget analysis separately are not novel approaches (these approaches have been used in previous studies to identify dominant MJO parameters and key MJO mechanisms), linking specific parameter modifications to specific MJO relevant mechanisms through the MSE budget is innovative and informative. Figs. 10 and 11 are particularly interesting as they connect the influence of parameter tuning on the impact of cloud-radiative feedbacks isolated to light-rain conditions. Below are a few specific comments and several technical comments that I encourage the authors to respond to.

Author Response: We sincerely thank the reviewer for the thoughtful and constructive comments. We have considered all the comments and revised the manuscript accordingly. In particular, we have provided additional analyses of the relationships between physical parameters and MJO metrics, investigated the role of *tau*, examined the regional sensitivity of cloud–radiation feedback, and clarified the distinction between cloud–radiation feedback and the suppressed convective anomalies associated with the MJO. Detailed responses to each comment are provided below (black indicates the reviewers' comments, blue indicates our responses, and green indicates the revised text in the manuscript).

Specific Comments

1. Sec. 2.3.1: Some more background information on the GLM equation is needed.

a. While the application of GLM to MJO performance is conceptually straightforward, it would likely benefit many readers to elaborate on this approach and its results. The cited Guo et al. (2014) paper presents a helpful summary in their section 3.1.1, and I'm wondering if the authors can produce a figure like Guo's Fig. 1.

Response: Thank you for this helpful suggestion. We agree that a clearer explanation of the GLM approach and its results would benefit readers. We have therefore expanded Section 2.3.1 to clarify the purpose of the GLM analysis and how the relative contributions of individual parameters are evaluated.

Following the visualization approach of Guo et al. (2014), we have also added two figures (Figs. R1 and R2) to illustrate the relationships between the 12 perturbed parameters and the two MJO metrics across the 128 PPE simulations. For each parameter, the 128 simulations are sorted into eight equally sized bins, each containing 16 members. The dots represent the bin-mean values of the MJO metric, while the error bars indicate the 25th–75th percentile ranges. Correlation coefficients are calculated using all 128 members, with red numbers indicating statistical significance at the 95% confidence level.

As shown in Figs. R1 and R2, *dmpdz* exhibits the strongest positive correlations with both the E/W ratio ($r = 0.50$) and PCC ($r = 0.52$). In contrast, *tau* and *ai* are negatively correlated with both metrics,

and these relationships are also statistically significant. Overall, the results support the identification of *dmpdz*, *tau*, and *ai* as the three leading parameters influencing MJO simulation skill.

The relevant text has been added to the revised manuscript (Lines 335–345), and the new figures are included as supplementary Figures S2 and S3.

"To complement the GLM analysis, we also examine the direct relationships between individual parameters and the MJO metrics (Figs. S2 and S3). For each parameter, the 128 PPE simulations are ranked by parameter value and divided into eight equally sized bins, each containing 16 simulations. The bin-mean MJO metrics and their 25th–75th percentile ranges are calculated, and Pearson correlation coefficients are evaluated using all 128 simulations. These relationships provide an intuitive illustration of individual parameter sensitivities, complementing the multivariate GLM results. Among the 12 parameters, *dmpdz* exhibits the strongest positive correlations with both the E/W ratio (r = 0.50) and PCC (r = 0.52). In contrast, *tau* and *ai* are negatively correlated with both metrics, with all these relationships significant at the 95% confidence level. These pairwise relationships are broadly consistent with the multivariate GLM results, which identify *dmpdz*, *tau*, and *ai* as the leading first-order contributors to MJO simulation skill."

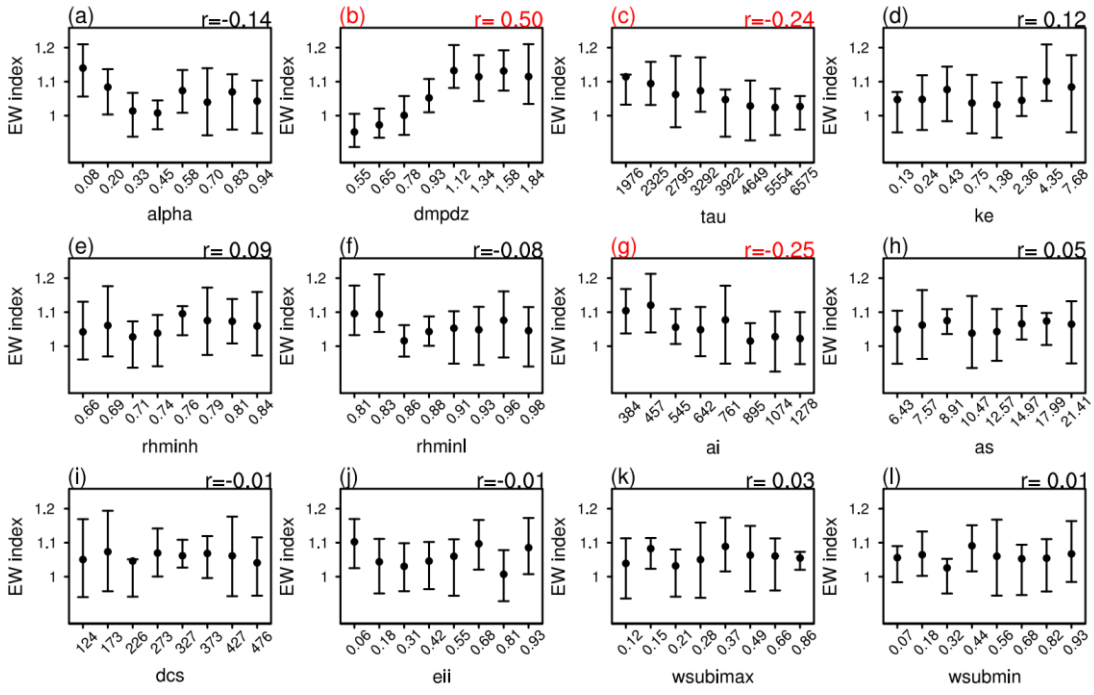


Figure R1. Relationships between the E/W index and the 12 perturbed physical parameters across the 128 PPE simulations. For each parameter, the simulations are ranked by parameter value and divided into eight equally sized bins, each containing 16 members. Dots indicate the bin-mean E/W

index, and the error bars represent the range between the 25th and 75th percentiles. The correlation coefficient between the E/W index and each parameter, calculated across all 128 simulations, is labelled on the upper-right corner of each panel, with red number indicating statistical significance at the 95% confidence level.

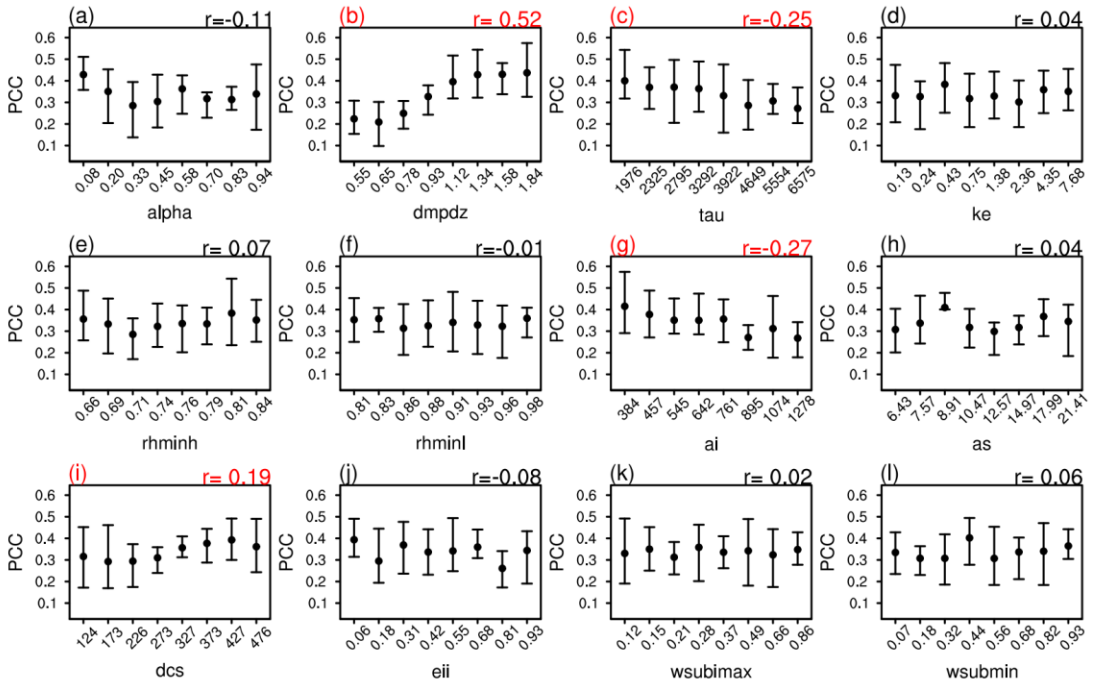


Figure R2. Same as Figure R1, but for the MJO propagation pattern correlation coefficient (PCC).

b. Please explain why two-way interaction terms are not considered in the GLM, though they are used in Eq. 1 of Guo et al. (2014). It may be of particular interest to understand interactions of tau with dmpdz and ai, given that DTN uses a strongly reduced tau value yet a maximized dmpdz to obtain the best MJO.

Response: We thank the reviewer for raising this important point. Our original GLM analysis included only linear terms because its primary purpose was to identify the dominant first-order parameter sensitivities across the 128-member PPE, rather than to construct a comprehensive nonlinear response model. Including all possible two-way interactions among the 12 parameters would introduce 66 additional terms, substantially increasing the model complexity relative to the available ensemble size.

Nevertheless, we agree that parameter interactions may be important, particularly between *dmpdz*

and *tau*. To examine this possibility, we have performed an additional GLM analysis that includes the linear, quadratic, and two-way interaction terms of the three dominant parameters identified in the original analysis (*dmpdz*, *tau*, and *ai*). Figures R3a and R3b show the relative contributions obtained from the original 12-parameter linear model, while Figs. R3c and R3d present the results from the extended second-order model involving these three parameters.

The results show that the linear effect of *dmpdz* remains the largest contributor to both MJO metrics. However, nonlinear effects are also evident in the fitted relationships. In particular, the *dmpdz* × *tau* interaction makes an appreciable contribution to the E/W ratio, while the quadratic term of *dmpdz* contributes notably to PCC. By comparison, the *tau* × *ai* interaction contributes relatively little.

We have added this analysis to the revised manuscript (Lines 321–334) and included the corresponding Figure R3b in the Supplementary Information.

"The original GLM (Eq. 1) includes only linear terms to identify the dominant first-order parameter sensitivities across the 128 PPE simulations. To further examine potential nonlinear effects and parameter interactions, we extend the analysis to include quadratic and two-way interaction terms for the three leading parameters identified by the linear GLM (*dmpdz*, *tau*, and *ai*). The quadratic terms account for nonlinear responses to individual parameters, while the two-way interaction terms describe how the influence of one parameter depends on the value of another. The extended model therefore includes three linear terms, three quadratic terms, and three two-way interaction terms. This additional analysis provides a complementary assessment of nonlinear parameter dependencies without introducing all possible interactions among the 12 parameters. As shown in Fig. S1, the linear term of *dmpdz* remains the largest contributor to both MJO metrics. However, the *dmpdz* × *tau* interaction contributes appreciably to the E/W ratio, while the quadratic term of *dmpdz* makes a notable contribution to PCC. These results suggest that the parameter dependence of MJO simulation skill may not be fully captured by an additive linear model. Nevertheless, the results continue to highlight *dmpdz*, *tau*, and *ai* as important parameters for further process-oriented investigation."

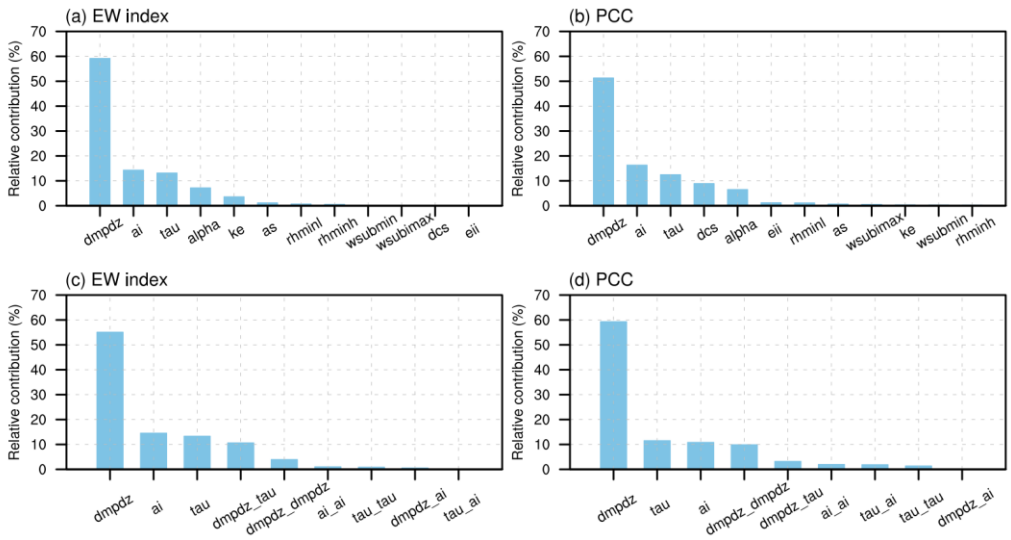


Figure R3. Relative contributions of physical parameter terms to the (a, c) E/W index and (b, d) MJO propagation PCC, estimated using GLM analyses. Panels (a, b) show the contributions of the 12 linear parameter terms in the original GLM, while panels (c, d) show the contributions of the linear, quadratic, and two-way interaction terms of the three leading parameters (*dmpdz*, *tau*, and *ai*) in the extended GLM. The relative contribution of each term is quantified by the increase in residual sum of squares when that term is excluded from the corresponding full model.

c. Parameters N and σ in Eq. (1) should be defined/quantified.

Response: Thank you for pointing this out. We have clarified the definitions of these symbols in the revised manuscript. In Eq. (1), n denotes the number of perturbed physical parameters, while N in $N(0,\sigma^2)$ denotes the normal distribution. To avoid confusion, we have revised $N(0,\sigma^2)$ to $\mathcal{N}(0,\sigma^2)$. Here, σ represents the residual standard deviation of the GLM.

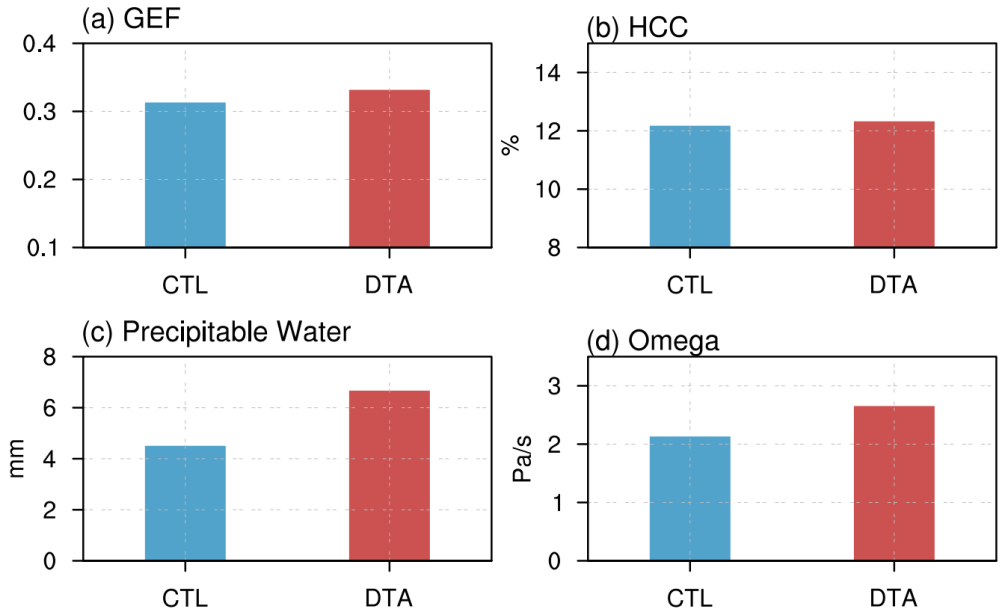
2. L524-532:

a. The longitudinal bounds selected to produce Figs. 9-11 are confusing. The authors initially describe the choice of longitudes 90°E-180°E as designed to encompass the eastward-propagation pathway of the MJO (L490-491). But based on Figs. 4 and 10, this seems to include both the MJO deep convective center (its eastern half) and the suppressed-convective eastern region toward which the MJO deep convective center is moving. Regarding the choice of using 90°E-180°E, this would

seem to include both the near-active MJO phase as well as the fully suppressed MJO phase. Is it known whether the results of Fig. 11 are influenced mainly by the more active MJO longitudes (say, 90°-135°E) or the suppressed longitudes (say, 135°E-180°E).

Response: We thank the reviewer for this thoughtful comment. We agree that the original description of the analysis domain may have caused some confusion. The longitude range of 90°E–180°E encompasses both the region near the MJO convective center and the region to its east when MJO convection is centered over the eastern Indian Ocean (EIO). However, it is important to distinguish the diagnostics used in Figs. 9–11. Figure 10 presents the regressed OLR and greenhouse enhancement factor (GEF) anomalies relative to the MJO convective phase over the EIO, whereas Figs. 9 and 11 examine cloud–radiation feedback under different precipitation anomaly conditions without explicitly separating MJO phases. Therefore, the western and eastern parts of the analysis domain should not be directly interpreted as representing fixed active and suppressed phases of the MJO.

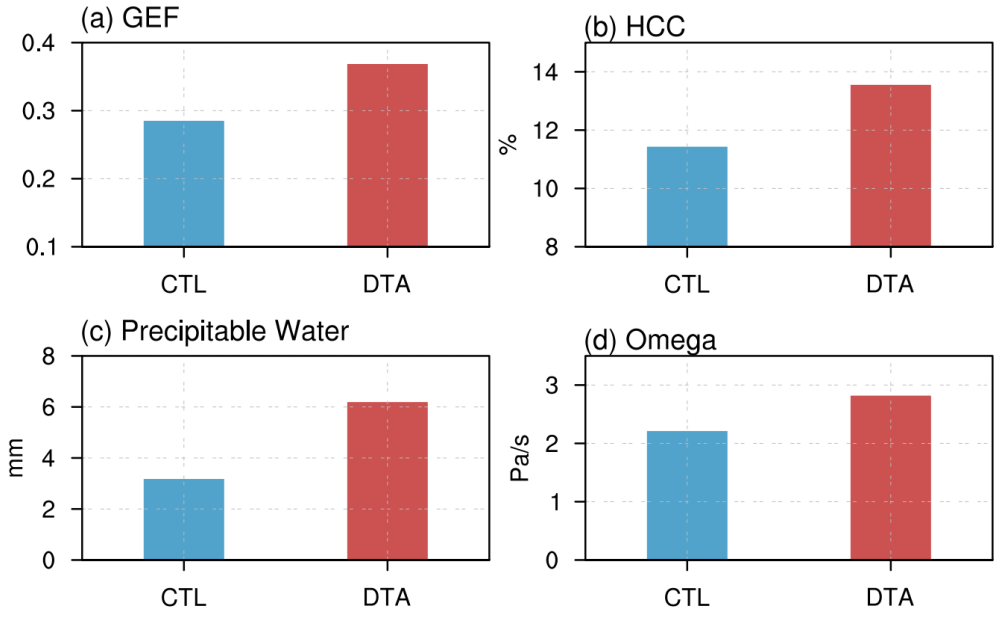
To address the reviewer's question, we repeated the analysis in Fig. 11 separately for the western (90°E–135°E) and eastern (135°E–180°) subregions, using the same weak precipitation anomaly regime (1–5 mm day^{-1}). The results are shown in Figs. R4 and R5. Compared with CTL, DTA exhibits larger GEF, greater precipitable water, and stronger upward motion in both subregions. However, the enhancements in GEF and high cloud cover (HCC) are considerably more pronounced in the eastern subregion, while the changes in the western subregion are relatively small. These results indicate that the enhanced cloud–radiation feedback in DTA is particularly evident over the eastern part of the analysis domain, rather than being dominated by the region closer to the MJO convective center.



164

165 **Figure R4.** Same as Fig. 11, but for the western subregion (15°S–10°N, 90°E–135°E). Bars show
166 (a) the greenhouse enhancement factor (GEF), (b) high cloud cover (HCC; %), (c) precipitable water
167 (mm), and (d) vertically averaged pressure velocity (1000–200 hPa) under weak positive
168 precipitation anomaly conditions (1–5 mm day^{-1}). Blue and red bars represent CTL and DTA,
169 respectively. Positive values in (d) indicate upward motion.

170



171

172 **Figure R5.** Same as Figure R4, but for the eastern subregion (15ºS–10ºN, 135ºE–180º).

b. For Figs. 10 and 11, the authors conditionally sample the data to retain only days when the precipitation anomaly is +1-5 mm/d ("light rain" anomalies), so intense rain grid cells are masked out. Fig. 11 indicates that DTA's improved MJO is associated with a higher GEF, HCC, precipitable water, and upward motion over the 90°E-180°E longitude band, compared to CTL. However, several previous studies have shown that MJO skill is higher for models that strongly *suppress* deep convection ahead of the MJO convective center, which allows atmospheric preconditioning to occur and instability to build. Is it the case from Figs. 9-11 that, although the large-scale convective suppression to the east of the MJO convective center is still happening, the light-rain events that do occur in that region are more vigorous (Fig. 11d) and result in a larger cloud-radiative feedback (Fig. 11a,b) that preconditions the atmosphere? Explaining this apparent distinction between the large-scale suppression of deep convection over the west Pacific, and the concurrent light-rain event characteristics in driving enhanced cloud-radiative feedbacks (as seen in Fig. 11), is important and should be clarified in the manuscript.

Response: We thank the reviewer for this insightful comment. We agree that the suppression of deep convection ahead of the MJO convective center plays an important role in atmospheric preconditioning and MJO propagation. However, the large-scale suppression of MJO convection and the characteristics of weak precipitation events represent different aspects of the convective system and are not necessarily contradictory.

As noted in our response to Comment 2a, Fig. 10 shows the MJO-related spatial structure obtained from regressions onto the EIO OLR index, whereas Fig. 11 examines the atmospheric conditions associated with weak positive precipitation anomalies (1–5 mm day^{-1}) without explicitly conditioning on MJO phase. The suppressed convective anomalies ahead of the MJO center reflect reduced convective activity on the intraseasonal scale, but do not imply a complete absence of weak precipitation or cloud formation. Therefore, the stronger upward motion under weak precipitation conditions in DTA (Fig. 11d) does not necessarily indicate a weakening of the large-scale convective suppression ahead of the MJO center.

Our results show that, under comparable weak precipitation anomaly conditions, DTA exhibits larger GEF, higher HCC, greater precipitable water, and stronger upward motion than CTL. These differences are consistent with more effective longwave cloud–radiation feedback associated with weak precipitation, which may favor MSE buildup and the subsequent development of MJO convection. However, because Fig. 11 is not conditioned on MJO phase, these results do not directly

establish whether the enhanced feedback occurs specifically within the suppressed region ahead of the MJO convective center or quantify its contribution to atmospheric preconditioning.

We have clarified the rationale for selecting the analysis domain and the distinction between precipitation-conditioned and MJO phase-conditioned diagnostics in Section 4.3 of the revised manuscript (Lines 539–542; Lines 588–593). The additional subregional analyses are presented in Figs. R4 and R5 to directly address the reviewer's concern.

3. L582-583:

It is stated that the influence of parameter *tau* remains unresolved, but couldn't this influence be highlighted by rerunning the DTA experiment by only changing *dmpdz* and *ai* (i.e., experiment "DA") and keeping *tau* at its default value? The resulting DTA–DA difference might elucidate the impact of the *tau* change on the simulation. This idea is mentioned in L588-589 and 593-595, and later in Sec. 6. A large number of simulations were conducted for this project, so it would seem reasonable to run one additional simulation to more cleanly identify the effects of *tau*. It is of particular interest to understand if minimizing *tau* artificially reduces biases (i.e., error compensation) that would otherwise degrade the mean state. That is, if *tau* is reverted to its default value in DTA, would the mean state worsen?

Response: We thank the reviewer for this constructive suggestion. We agree that a DA experiment, with *dmpdz* and *ai* fixed at their DTA values and *tau* restored to its CTL value, would provide a more direct assessment of the effect of *tau*. However, given the computational cost of an additional long-term CAM6 simulation, we instead explored this issue using the existing PPE simulations.

Specifically, we selected three pairs of PPE members with higher *dmpdz* and lower *ai* than in CTL, but contrasting *tau* values within each pair: members 68 and 74, 57 and 53, and 26 and 63 (Table R1). These configurations follow the directions of the *dmpdz* and *ai* adjustments in DTA, although their parameter values are not identical to those in DTA or between paired members.

Figures R6 and R7 compare the MJO characteristics across these three pairs. In each pair, the member with smaller *tau* (68, 57, or 26) exhibits more coherent eastward propagation of OLR anomalies and stronger eastward-propagating spectral power within the MJO band than its

counterpart with larger *tau* (74, 53, or 63). These consistent differences support the negative association between *tau* and MJO simulation skill identified by the GLM analysis.

To examine the accompanying differences in mean precipitation, we compared MJO propagation skill and mean precipitation metrics across the same pairs (Fig. R8). Over the tropics, members with smaller *tau* consistently exhibit higher MJO-PCC and lower mean precipitation RMSE, whereas the differences in mean precipitation PCC are relatively small (Figs. R8a, b). Over the Northern Hemisphere midlatitudes, the differences in both mean precipitation metrics are also small (Figs. R8c, d). Thus, in these selected comparisons, better MJO propagation skill is accompanied by reduced tropical mean precipitation error.

Although *dmpdz*, *ai*, and other parameters also differ within each pair, the consistent results support an association between smaller *tau*, improved MJO skill, and lower tropical precipitation RMSE. A controlled DTA–DA experiment would still be needed to isolate the contribution of *tau* and determine whether error compensation plays a role. We have added these comparisons to Section 4.4 and explicitly acknowledged their limitations, with the supporting table and figures included in the Supplement (Lines 645–658).

Table R1. Values of the 12 perturbed physical parameters for three pairs of PPE members: 68 and 74, 57 and 53, and 26 and 63.

PPE member	alpha	**dmpdz**	**tau**	ke	rhminh	rhminl	**ai**	as	dcs	eii	wsubimax	wsubmin
68	0.752656	**1.775376**	**2629.652**	0.184342	0.695313	0.884609	**402.9162**	6.601417	478.125	0.289773	0.429351	0.617188
74	0.568906	**1.628027**	**4822.803**	2.458244	0.707813	0.920234	**439.3833**	8.560978	453.125	0.726836	0.278813	0.929688
57	0.117187	**1.325237**	**2284.292**	3.398208	0.753125	0.933594	**463.8328**	8.109712	206.25	0.734641	0.138237	0.078125
53	0.178437	**1.718619**	**3522.859**	0.805842	0.665625	0.897969	**425.3366**	17.68741	281.25	0.672203	0.378552	0.765625
26	0.591875	**1.915207**	**2898.883**	6.493816	0.80625	0.960313	**365.4958**	9.437473	212.5	0.906344	0.805842	0.34375
63	0.484687	**1.575981**	**3841.705**	6.042964	0.728125	0.862344	**390.0354**	13.63886	256.25	0.360016	0.184342	0.703125

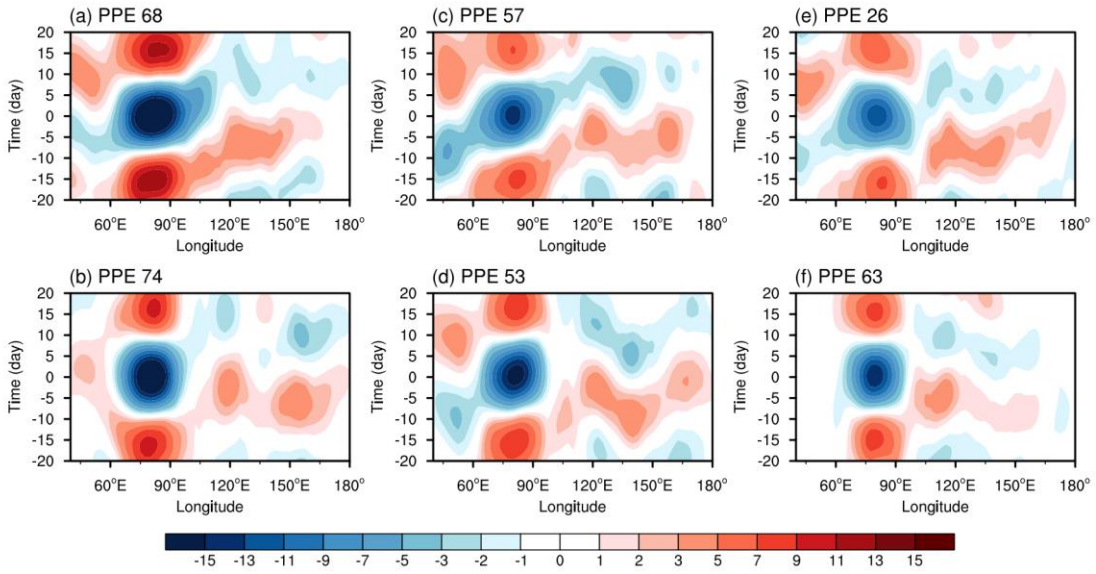


Figure R6. Lag-regression diagram of 10ºS–10ºN averaged OLR anomalies (units: W m^{-2}) by regressing OLR onto the intraseasonal OLR anomalies averaged over the eastern Indian Ocean (10ºS–10ºN, 75º–95ºE). Results are shown for three pairs of PPE members: (a, b) 68 and 74, (c, d) 57 and 53, and (e, f) 26 and 63.

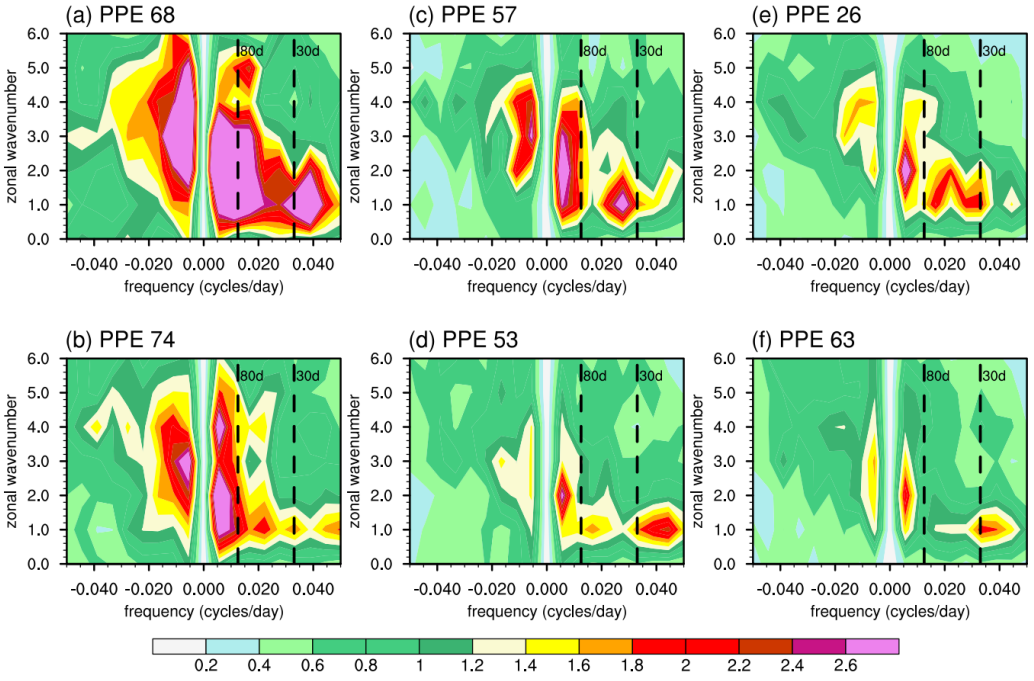
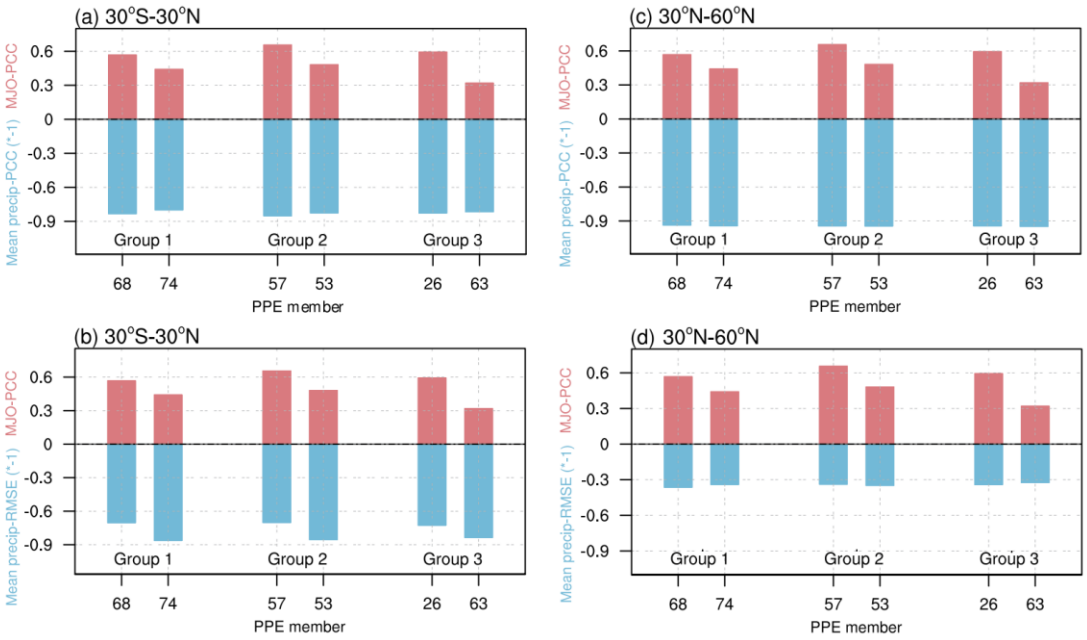


Figure R7. Zonal wavenumber-frequency power spectra of November–April OLR anomalies averaged over 10ºS–10ºN for three pairs of PPE members: (a, b) 68 and 74, (c, d) 57 and 53, and (e, f) 26 and 63.



261

262 **Figure R8.** Comparison of MJO propagation skill (red bars) and mean precipitation metrics (blue
263 bars) across three pairs of PPE members. Mean precipitation skill is evaluated by (a, c) PCC and (b,
264 d) root-mean-square error (RMSE; units: mm day^{-1}) over the (a, b) tropics (30°S–30°N, 0°–360°)
265 and (c, d) Northern Hemisphere mid-latitudes (30°N–60°N, 0°–360°). The mean precipitation
266 metrics are multiplied by −1.

267

268 **Technical Corrections**

269 **1. L50:** Klotzbach (2014) is another good paper to cite here, related to MJO impacts on tropical
270 cyclones worldwide:

271 Klotzbach, P. J., 2014: The Madden–Julian Oscillation's Impacts on Worldwide Tropical Cyclone
272 Activity. J. Climate, 27, 2317–2330, https://doi.org/10.1175/JCLI-D-13-00483.1.

273 **Response:** We have added the reference to the revised manuscript.

274

275 **2. L60-61:** Sensitivity of the MJO to the deep convection parameterization has been known for a
276 long time. Consider adding this paper, which notes that MJO skill differs based on deep convective
277 scheme in a model intercomparison:

278 Slingo, J.M., Sperber, K.R., Boyle, J.S. *et al.* Intraseasonal oscillations in 15 atmospheric general
279 circulation models: results from an AMIP diagnostic subproject. *Climate Dynamics* **12**, 325–357
280 (1996). https://doi.org/10.1007/BF00231106.

281 **Response:** We have incorporated the reference into the revised manuscript.

282

283 **3. L202-203:** It's recommended to cite this statement using:

284 Zhang, C., and M. Dong, 2004: Seasonality in the Madden–Julian Oscillation. *J. Climate*, **17**, 3169–
285 3180, https://doi.org/ 10.1175/1520-0442(2004)017<3169:SITMO>2.0.CO;2.

286 **Response:** The suggested reference has been included in the revised manuscript.

287

288 **4. L212:** "*j*-th parameters" —> "*j*-th parameter"

289 **Response:** The error has been corrected.

290

291 **5. L230-231:** Is Qr derived from a vertical integral of multi-level longwave (QRL) and shortwave
292 (QRS) radiative heating rates, or the difference in single-level model-top (FLNT, FSNT) and surface
293 (FLNS, FSNS) heating rates?

294 **Response:** The column-integrated radiative heating term (Qr) is calculated from the difference
295 between the net radiative fluxes at the top of the atmosphere and the surface. We have clarified this
296 detail in the revised manuscript (Lines 225–226).

297

298 **6. L278 & 352:** regression —> regressing

299 **Response:** Corrected as suggested.

7. Fig. 4: Are negative column MSE contours omitted from the figure? If so, this should be stated in the caption.

Response: Yes, the negative column MSE contours are omitted in Fig. 4. We have clarified this in the figure caption.

8. L369-371: I have no doubt the authors carefully considered their decision to project *model*-derived column MSE budget terms onto *observation*-derived column MSE and MSE tendency patterns to produce Fig. 5. However, I am wondering about the validity of this approach. It would seem that this approach could potentially result in comparing a MSE budget term that is physically inconsistent with the column MSE and MSE tendency pattern onto which it is projected. This would seem to be particularly true in the case of the CTL simulation, which shows column MSE and MSE tendency patterns that differ considerably from OBS in Fig. 4. It would benefit the manuscript to further justify their approach.

Response: Thank you for raising this important concern. We chose to project the simulated MSE budget terms onto the observed MSE and MSE tendency patterns for the following reasons:

(1) The primary purpose of this study is to identify which changes in the simulated physical processes help explain the improved MJO performance in DTA relative to CTL. We therefore use the observed MSE and MSE tendency patterns as common references, allowing a direct comparison of the projection coefficients between CTL and DTA. In contrast, projecting the MSE budget terms from each experiment onto its own MSE and MSE tendency patterns would yield coefficients referenced to different spatial structures, making it difficult to directly assess their correspondence with the observed MJO patterns.

(2) The projection coefficients quantify how strongly each simulated MSE budget term projects onto the observed MSE and MSE tendency patterns. For example, Figure 2 shows that the CTL fails to reproduce the observed eastward propagation of the MJO. Even if meridional MSE advection plays an important role in CTL's simulated MJO propagation, this does not necessarily mean that it supports realistic eastward propagation. A weaker projection onto the observed MSE and MSE

tendency pattern therefore indicates a smaller component aligned with that reference pattern, rather than a smaller contribution to the MSE budget within CTL itself.

9. Fig. 6 (and L239): Connecting the decomposed vadv budget terms between Eq. 5 and Fig. 6 could be improved. Consider either adding number labels to each term on the rhs of Eq. 5, or explicitly labeling each numbered tickmark in Fig. 6 with the budget term.

Response: Thank you for this suggestion. We have added numerical labels to the terms on the right-hand side of Eq. (5) to establish a clearer correspondence with Fig. 6.

10. L401-402: It is recommended to specify that this term is the "intaseasonal anomaly of the column-integrated intraseasonal meridional advection of the low-frequency background MSE".

Response: We have revised the description of this term ($-\langle v'\partial m/\partial y\rangle'$).

11. L407: facillates —> facilitates.

Response: Corrected as suggested.

12. L411: Add "not shown"?

Response: Thank you for the suggestion. We have added "not shown" to clarify that the meridional gradient of background MSE is not presented.

13. L447-448: Is this statement in reference to a particular longitudinal range in Fig. 8b? It seems to be most relevant to the Indian Ocean basin.

Response: We have clarified that this statement primarily refers to the Indian Ocean and western Pacific region.

14. L459: HCC has not yet been defined.

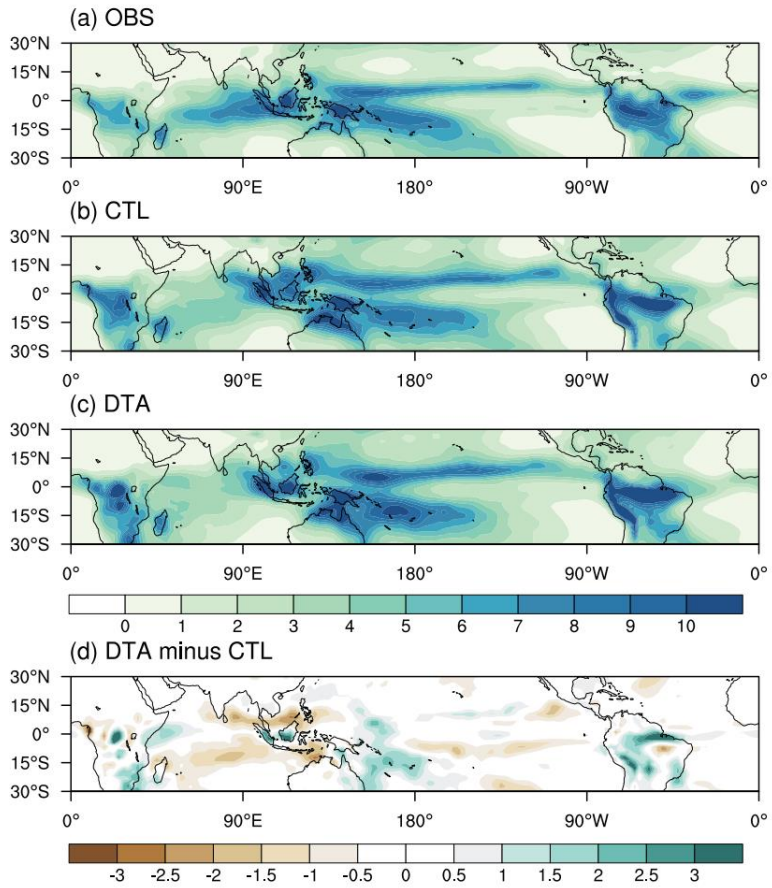
Response: We have defined "high cloud cover (HCC)"at its first occurrence.

15. L581: 12d —> 11d.

Response: Corrected.

16. L613-614: The "weak negative anomalies" in time mean precipitation aren't able to be seen because the multi-panel color bar in Fig. 12 is positive-only.

Response: Thank you for careful reading. We have revised the color bar to display both positive and negative precipitation differences (Fig. R9) and updated the corresponding description in the revised manuscript.



364

365 **Figure R9.** November–April mean precipitation (units: mm day^{-1}) for (a) observations, (b) the CTL
366 experiment, (c) the DTA experiment, and (d) the DTA−CTL difference.

367

368 **17. L673-675:** It would be very helpful to add figure references, where appropriate, to the sentences
369 in the Conclusions section. The sentence L673-675 is one good example, where a reference to Fig.
370 8a could be added.

371 **Response:** Thank you for this helpful suggestion. We have added relevant figure references
372 throughout the Conclusions section.

373

374 **18. L687:** "higher" —> "more.

375 **Response:** Corrected as suggested.